Crystal structure of high–density Fe_{56} cluster $Nd_2Fe_{14}B$ under high pressure

Takayuki Tajiri[1] and Masaki Mito[2]

[1] Faculty of Science, Fukuoka University, Fukuoka 814-0180, Japan

[2] Graduate School of Engineering, Kyushu Institute of Technology, Kitakyushu 804-8550, Japan

Abstract

$Nd_2Fe_{14}B$ is a high-density Fe cluster containing 56 Fe atoms in one unit cell. We investigated the crystallographic structure of an isotropic $Nd_2Fe_{14}B$ magnet comprising nanocrystals of a size of ~30 nm at pressures up to 2 GPa. The results of X-ray diffraction measurements using Rietveld refinement revealed the displacements of each Fe atomic site in the Fe cluster, Nd, and B atomic sites. The lattice constants, *a* and *c*, of tetragonal symmetry decreased proportionally with external pressure, whereas the shrinkage ratio for both *a* and *c* changed at approximately 0.5 GPa. However, each atomic position exhibited non-monotonic pressure dependence. The trend of displacement of atomic positions changed at a characteristic pressure of 0.4 ± 0.1 GPa. When exceeded, most atoms shifted to the direction opposite their displacement at lower pressures. Thus, they exhibited restoration tendencies toward the positions at ambient pressure. The bond angles and bond lengths among Nd, Fe, and B atoms also exhibited characteristic pressure dependences. As pressure increased, the basal triangle of the trigonal prism in the Fe cluster layers distorted up to ~0.5 GPa, whereas the strain of the trigonal prism gradually reduced to just above 0.5 GPa. The atomic position of the heaviest Nd atoms was a key structural parameter use to characterize the change.

I. Introduction

$Nd_2Fe_{14}B$ is the main phase of the superior Nd-Fe-B permanent magnets with a high coercive field of a few 1 T levels and a large energy product $(BH)_{max}$ ~ 500 kJ/m^2 [1-5]. The ratio of rare-earth Nd to transition metal Fe is 1:7. From a scientific viewpoint, $Nd_2Fe_{14}B$ is a high-density Fe cluster system in which there are 56 Fe atoms in one unit cell [5,6]. Accordingly, there is hardly any space between constituent atoms. There are various Fe sites and exchange interaction paths. The ferromagnetic transition temperature (T_C) of $Nd_2Fe_{14}B$ is generally recognized as 586 K [1,5,7–9], whereas there has been a serious problem that the performance of high-Hc permanent magnets deteriorated due to temperature changes. Thus, changes in temperature bring about changes in performance. In actual use, there are two types of real Nd-Fe-B magnets: isotropic bond and sintered. As an application for free shaping, rapid solidification via a melt-spinning produces “an isotropic bond magnet” with a grain size of less than 1 μm. For grain sizes less than 0.3 μm, the single magnetic domain structure is stabilized [2,10,11]. In sintered magnets, the insertion of Dy at the Fe site is an effective method of enhancing H_c at around 500 K [12]. To understand and improve the permanent magnet performance of sintered magnets, experimental and theoretical studies on the origins of high H_c at the domain level [13,14] have been conducted [10,11,15]. The magnetic anisotropy required for permanent magnets generally originates from crystalline anisotropy, owing to spin–orbit coupling and shape anisotropy. The spin–orbit coupling of 4*f* electrons of rare earths is one-order larger than that of Fe-3*d* electrons. The hybridization between spin magnetic moments of Fe-3*d* and Nd-5*d* electrons and this effect are correlated with the orbital magnetic moment of Nd-4*f* electrons via the exchange interaction between spin magnetic moments of Nd-5*d* and Nd-4*f*. Differences in rare-earth elements bring about changes in magnetic anisotropy [16]. The interfaces between the main and grain boundary phases also play an important role in realizing effective anisotropy [10,11].

Our interest is in the magneto-structural correlation in the high-density Fe cluster system, including heavy Nd and light B. We conducted a hydrostatic pressure experiment using pressure (P) as continuous external perturbation to continuously manipulate the crystal structure. There have been experimental reports on hydrostatic pressure experiments, the effects on T_C of $Nd_2Fe_{14}B$. They primarily on changes in T_C [17,18]. According to an experiment by Kamarad *et al.* (1987), the change in T_C against the pressure

for dT_C/dP = -26.5 K/GPa [17]. In amorphous $Nd_2Fe_{14}B$ [$T_C(P = 0)$ = 422 K], dT_C/dP = -48 K/GPa [18]. In 2015, the pressure effect on H_c was investigated via magnetization curve measurements at pressures up to 9.3 GPa [19]. In X-ray diffraction (XRD) measurements, a reduction in crystallinity was recognized at pressures above ~2 GPa, below which H_c linearly increased with pressure. However, because studies on each atomic position have been unsuccessful, discussions on magneto-structural correlation, including changes in magnetic anisotropy, have been insufficient.

We therefore focus on the interactive displacement of each atom in a highly filled Fe-cluster with Nd and B until the beginning of crystallinity reduction. The spin-orbit coupling changes under pressure because of the change in hybridization between Fe-3*d* and Nd-5*d*, and it is difficult to understand the physical origins of this change. Indeed, the atomic level of displacement at high pressures must be complicated owing to the highly filled crystal structure. Information on the atomic positions of constituent elements has yields important knowledge on the magneto-structural correlation of a highly filled Fe-cluster, and this knowledge would be useful for designing a superior permanent magnet at the atomic level.

$Nd_2Fe_{14}B$ has a tetragonal symmetry (space group $P4_2/mmm$) containing four formula units: 68 total atoms (8 Nd, 56 Fe, 4 B), as shown in Fig. 1 [3]. There are six crystallographically distinct Fe sites, two Nd sites, and one B site. The $Nd_2Fe_{14}B$ unit cell comprises eight layers repeating along the *c* axis. The Nd atoms occupy 4*g* and 4*f* sites, termed Nd1 and Nd2, respectively. The B site is 4*f*. The *z*-coordinate of Nd and B is 0 or 0.5, in the unit cell. Between their Nd-and-B planes at z = 0 and 0.5, most Fe atoms form somewhat distorted hexagonal nets. The Fe atoms occupy 16*k*, 16*k*, 8*j*, 8*j*, 4*e*, and 4*c* sites, termed Fe1, Fe2, Fe3, Fe4, Fe5, and Fe6, respectively. The near-neighbor Fe-Fe distances in the structure are between 2.4 and 2.8 Å. The B atoms play an important role in bonding, because they occupy the centers of the trigonal prisms formed by six nearly neighboring Fe atoms [3, 4, 5]. Three Nd atoms (two 4*g*-Nd and one 4*f*-Nd) are bonded to each B atom via the three vertical prism faces [13]. B atoms contribute to the stabilization of the structure and substantially reduce the magnetic moment of neighboring Fe atoms via a hybridization interaction. The Fe-3*d* states couple with the Nd-4*f* states via hybridization between the Fe-3*d* and Nd-5*d* electrons [13]. The Fe-3*d* electrons mainly determine the density of the state near Fermi energy, E_F. The Fe-3*d* magnetism in $Nd_2Fe_{14}B$ is understood in terms of itinerant magnetism of

Fe-3*d* electrons. Depending on the distances between Fe and B atoms, the Fe atoms at the 8*j* (Fe4) and 4*e* (Fe5) sites have the largest and smallest magnetic moments, respectively [20]. In this study, we performed powder XRD measurements, and the crystallographic structure of the main phase of the Nd-Fe-B magnet was obtained using Rietveld analysis under a hydrostatic pressure of ~2 GPa. We observed that the structural deformation under pressure was representatively monitored with changes in the position of the lightest atom, B.

II. Experiment

To determine the crystal structure via Rietveld analysis, we used the polycrystalline of the $Nd_2Fe_{14}B$ (exact chemical formula is $Nd_{2.0}Fe_{14.1}B$) isotropic bond magnet comprising nanoparticles having a particle size of ~60 nm and a crystallite size of ~30 nm [19]. The small particle size of $Nd_2Fe_{14}B$ powder provides good Debye–Scherrer rings without spots and improves the accuracy of Rietveld analysis. The same isotropic bond magnet was used in the high-pressure experiment (up to 9.3 GPa) [19]. At 300 K, for $P < 4$ GPa, H_c increased linearly against pressure. T_C decreased as $dT_C/dP = -17.8$ K/GPa.

Powder XRD measurements under pressure were carried out at room temperature using a synchrotron radiation X-ray diffractometer and a Debye-Scherrer camera at a beamline of BL-8B at the Photon Factory of the Institute of Materials Structure Science, High Energy Accelerator Research Organization. The wavelength of the incident X-ray, 0.88249 Å, was calibrated using the XRD pattern of CeO_2 powder. Hydrostatic pressure was applied using a CuBe diamond anvil cell with a 0.3 mm-thick gasket made of CuBe. The polycrystalline $Nd_2Fe_{14}B$ powder was placed inside a sample hole of 0.4 mm diameter with a ruby and fluorinated oil (FC77, Sumitomo 3M) as the pressure-transmitting medium [21]. The pressure value was estimated by measuring the fluorescence of the ruby located in the sample cavity [22]. The Rietveld analysis program, RIETAN-FP [23], was used to analyze the XRD measurement results.

III. Experimental results

We obtained powder XRD patterns for $Nd_2Fe_{14}B$ at room temperature up to 1.95 GPa. The XRD patterns maintained a tetragonal symmetry with a space group, $P4_2/mnm$. The profiles shifted to the

higher-angle side with increasing pressure. When we conducted Rietveld analysis for a series of data, the XRD patterns were refined using the $P4_2/mnm$ space group in the considered pressure region. Figure 2 shows the powder XRD patterns and Rietveld analysis results at ambient pressure converged in an authentic level with an R factor, R_{wp}=6.957 and R_e=2.535. The effective error appeared in the atomic coordinate of light B atom. Table I shows the structural parameters, lattice constants, and all atomic sites refined by Rietveld analysis at ambient pressure. XRD patterns at high pressure were also reproduced with similar R factors. There was no sign of reduction in crystallinity in the pressure region. Figure 3 shows the pressure dependence of lattice constants a (a) and c (b), estimated by Rietveld analysis. The lattice constants, a and c, decreased with almost the same contraction ratio, $a(P)/a(P=0)$ and $c(P)/c(P=0)$. This indicates that the crystallographic structure of $Nd_2Fe_{14}B$ was isotropically compressed up to 1.95 GPa, as shown in Fig. 3(c). The ratio of lattice constants c to a maintained a constant value, c/a = 1.388. As pressure increased, both a and c decreased linearly, and the trend of the pressure dependence of the lattice constants changed at ~0.5 GPa. The compression coefficients of both a and c axes to pressure, da/dP and dc/dP, reduced more than ~0.5 GPa. For $P < 0.5$ GPa, the values of da/dP were -0.0275 Å/GPa, and dc/dP were -0.0343 Å/GPa, respectively, whereas, for $P > 0.5$ GPa, the values of da/dP were -0.0166 Å/GPa and dc/dP were -0.0231 Å/GPa, respectively. The values of the compression coefficient for $P > 0.5$ GPa were approximately 60% that for $P < 0.5$ GPa. The pressure dependence of the unit-cell volume also exhibited an inflection point around $P = 0.5$ GPa. Furthermore, the values of dV/dP are -8.466 $Å^3$/GPa and -5.266 $Å^3$/GPa, for $P < 0.5$ GPa and $P > 0.5$ GPa, respectively. Li *et al.* reported the shock experimental inertia of $Nd_2Fe_{14}B$ to be within 18–78 GPa [24], indicating that the deviation of $V(P)/V(0)$ against P was about -3.2×10^{-3} /GPa. The value is a half of the present result: -6.5×10^{-3} /GPa.

All atomic positons were estimated via Rietveld analysis at both high and ambient pressures. Figure 4(a) shows the pressure dependence of the x-coordinate for two individual Nd sites (Nd1 and Nd2), which are special positions, 4*g* and 4*f*, for Nd1 and Nd2, respectively. The tendency of the displacement for two Nd atoms differed from each other. The value of the x-coordinates for Nd1 and Nd2 reached their minimum at ~0.2 and ~0.5 GPa, respectively. Both Nd sites shifted to the opposite direction above the pressures. Thus, the Nd atoms approached the atomic position at ambient pressure. Figure 4(b) shows

the schematics of the displacement tendency of the Nd atomic positions in the *ab*-plane. As pressure increased, the two Nd sites shifted outward in the *ab*-plane below ~0.5 GPa and subsequently inward above ~0.5 GPa. In fact, the bond length between Nd1 and Nd2 stretched to below 0.3 GPa, despite a decrease in the lattice constants, as shown in Fig. 3. For $P > 0.3$ GPa, the bond lengths reduced with increasing pressure, as shown in Fig. 4(c).

The Fe network of $Nd_2Fe_{14}B$ comprises six individual iron-sites; two general positions 16*k* for Fe1 and Fe2, and four special positons, 8*j*, 8*j*, 4*e*, and 4*c* for Fe3, Fe4, Fe5, and Fe6 respectively. Figure 5 shows the pressure dependence of the respective coordinates for the Fe atomic positions, *x*(Fe1), *y*(Fe1), *x*(Fe2), *y*(Fe2), *x*(Fe3), *z*(Fe3), *x*(Fe4), *z*(Fe4), and *z*(Fe5). The trends of displacement in each Fe site changed at approximately 0.3–0.5 GPa, which was like those of the Nd sites. The tendency of displacement of Fe2 in particular was very similar to that of Nd2, owing to the absence of Nd1 atoms around the Fe2 site. Figure 6 shows the schematics of the tendency of displacement of the Fe atomic position of projection in the *ab*-plane and along the *c*-axis below/above 0.5 GPa. The Fe atoms near the center of the unit cell in the *ab*-plane shifted inward, whereas the Fe atoms near the edge moved outward at below ~0.5 GPa. However, for $P > 0.5$ GPa, each Fe atom moved in the opposite directions. Thus, each Fe atom exhibited the tendency to return its original position at ambient pressure. These results indicate that Fe sites were remarkably influenced by the shift of Nd sites. Figure 7 shows the pressure dependence of the respective interatomic distances between the different Fe sites around the Nd sites. The results indicate that the Fe cluster layer, comprising Fe1-Fe5, as shown in Fig. 1, exhibited expansion along the *c*-axis by the displacement of each Fe sites, despite the contraction of lattice constants below ~0.5 GPa, as shown in Fig. 8. This means that the interlayer distance between the Nd plane and the Fe cluster layers contracted. However, above 0.5 GPa, the displacement of each Fe site was oriented toward the opposite direction, suggesting the constriction of the extended Fe cluster layer. Thus, the manner of the shrinkage of crystallographic structure changes at ~0.5 GPa, as shown in Fig. 3, and the degrees can be attributed to the changes in the tendency of displacement at each Fe site.

$Nd_2Fe_{14}B$ contains the trigonal prisms formed by the three nearest Fe atoms in the Fe cluster as shown in Fig. 9(a). The B atoms occupy the centers of the trigonal prism, which are structural units linking the Fe planes above and below those containing Nd and B atoms, located in $z = 0$ and 0.5. The

trigonal prisms appear in pairs having a common Fe5-Fe5 edge and share two Nd1 atoms. The prism faces participate in completing the hexagonal Fe nets over the square basal units, as shown in Fig. 6(a). Figures 9 (b–f) and 10 (a–d) show the pressure dependences of the interatomic distances and bond angles between neighboring atoms forming a trigonal prism. The isosceles triangle formed by two Fe2 and one Fe5 atoms exhibited changes in distortion tendencies at ~0.5 GPa. Below 0.5 GPa, as the pressure increased, the triangle became more distorted from equilateral. The Fe2-Fe5-Fe2 bond angle increased, whereas the bond angle of Fe5-Fe2-Fe2 decreased from 60°. The bond lengths of the triangle exhibited opposite behaviors between the Fe2-Fe2 and Fe2-Fe5 distances. However, for $P > 0.5$ GPa, the two bond angles and two bond lengths moved toward the values at ambient pressure as pressure increased. Thus, the strain of the triangles reduced, and the shape of the triangle resembled an equilateral triangle. For $P < 0.5$ GPa, as the pressure increased, the bond angles of Nd1-B-Nd2 and Nd1-B-Nd1 decreased and increased. The bond lengths for Nd2-B and Nd1-B increased and decreased, respectively, with increasing pressure. For $P > 0.5$ GPa, the two bond angles exhibited the opposite behaviors of those for $P < 0.5$ GPa, which were similar to those of the angles of the triangles formed by two Fe2 and one Fe5 atoms, as shown in Fig. 9. The changes in the two Nd-B-Nd bond angles, including the heaviest Nd, is thought to have induced the distortion of the triangle formed by the Fe atoms.

The *x*-coordinate of B atoms decreased slightly with increasing pressure and saturated above 0.5 GPa. This is represented in Fig. 11, which shows pressure dependencies of bond length between B and Fe atoms. These bond lengths also exhibited an inflection point at around 0.5 GPa. Figures 11(a) and (d) suggested that the relative position of B atoms in the triangle shifted toward the center of the triangular prism below 0.5 GPa and shifted to the side face closest to the Fe atom at above 0.5 GPa.

IV. Discussion

The results of the crystal structure analysis demonstrated that the lattice constants decreased as the pressure increased, whereas the non-monotonic displacement of all the atomic positions occurred because of high atomic filling. The pressure dependences of the lattice constants and atomic positions exhibited pronounced changes at around 0.3–0.5 GPa. The experimental results indicated that, as a whole, the atomic locations of Fe and B translated according to the movement of Nd sites. For $P < 0.5$

GPa, the Nd atoms displaced each Fe site outward from the *ab*-plane. For $P > 0.5$ GPa, when the Nd atoms shifted inward of the *ab*-plane, the Fe and B atoms moved to the blank space formed by the movement of Nd atoms. The displacements of Fe2 and B atoms located far from Nd1 and close to Nd2 were attributed to the movement of Nd2 atom. However, the Fe1, Fe2, and Fe4 atoms located between the Nd1 and Nd2 sites moved under the influence of the displacement of both the Nd1 and Nd2 sites. The relative thickness of the Fe cluster layer in the unit cell was strongly influenced by displacement of Nd1 site. Therefore, it increased under lower pressure and decreased under higher pressure. The external pressure induced the translation of the atomic position. The shifts of each atom folded back in the atomic position at an ambient pressure above 0.5 GPa. It has been speculated that the crystallographic structure at ~0.5 GPa is quasi-stable under hydrostatic compression and that additional pressurization induces the forcible shift of each atom from its stable condition above 0.5 GPa.

Under high pressure, the magnetic properties of the $Nd_2Fe_{14}B$ (e.g., coercive field, saturation magnetization, and Curie temperature) depend on external pressure [17–19]. The Curie temperature and saturation magnetization decreased and the coercive field increased with increasing pressure. The magnetic moment of $Nd_2Fe_{14}B$ was reduced under pressure [19]. The magnetic moments for Fe atoms are theoretically known to depend on their distance from the B atoms [20]. The B atoms contribute to the stabilization of the structure and substantially reduce the magnetic moment of the neighboring Fe atoms through a hybridization interaction [20]. Depending on the distance from the B atoms, the calculated and experimental magnetic moments for Fe4 and Fe5 sites were 2.69–3.40 μ_B and 1.91–2.28 μ_B, respectively [20]. The current results reveal that external pressure changes the stability of the structure and magnetic moments. The trend on displacement of constituting elements for $P < 0.5$ GPa is contrary to that for $P > 0.5$ GPa. For $P > 0.5$ GPa, the stability of the structure returns to those at ambient pressure, because the pressure dependences of the bond length and the atomic coordinate exhibited opposite behaviors at pressures below 0.5 GPa. The current results suggest that the magnetic moments for each Fe atom should change under pressure, resulting in a change in the total magnetic moment. Thus, as a first step, it is desirable to calculate the magnetic moment based on the crystal structure under pressure. The final goal is to understand the pressure dependence of the coercive field, saturation magnetization, and Curie temperature.

V. Summary

We investigated the hydrostatic pressure effects on the crystallographic structure of $Nd_2Fe_{14}B$ using a powder XRD experiment with Rietveld analysis. The experimental results indicated the changes in the lattice constants and atomic coordinates under high pressure. The pressure dependences of lattice constants and atomic coordinates are non-monotonous, and the contraction of the lattice constants abated above approximately 0.5 GPa. The tendency of displacement of atomic coordinates changes at approximately 0.3–0.5 GPa. The shift of Nd atoms induces the deformation of Fe cluster under high pressure. The changes in the bond angles and lengths among Nd, Fe, and B atoms in a trigonal prism formed by Fe atoms indicated that the basal plane of trigonal prism exhibited a tendency to distort as the pressure increased to about 0.5 GPa. However, above 0.5 GPa, the trend of displacement of atomic positions changed, and the strain of triangle reduced with increasing pressure. The shift of each atom folded back in the atomic position at ambient pressures above 0.5 GPa. This behavior suggests that the crystallographic structure at around 0.5 GPa is quasi-stable under hydrostatic compression. The changes in the bond lengths between Fe and B induced modulation of the magnetic moments for each Fe site and overall magnetic moment for $Nd_2Fe_{14}B$. It is presumed that the changes in the crystallographic structure induced the degradation of magnet performance, such as the reduction of coercive field and saturation magnetization under high pressure.

Acknowledgments

This work was supported by MEXT KAKENHI [Grantin-Aid for Scientific Research (B) (No. 26289091) and Grant-in-Aid for Scientific Research on Innovative Areas “Bulk Nanostructured Metals” (No. 25102709)]. Authors acknowledge Magnequench International for supplying the $Nd_{2.0}Fe_{14.1}B$ isotropic bond magnets.

References

[1] M. Sagawa, S. Fujimura, N. Togawa, H. Yamamoto, and Y. Matsuura,J. Appl. Phys. **55**, 2083 (1984).

[2] J. J. Croat, J. F. Herbst, R. W. Lee, and F. E. Pinkerton, J. Appl. Phys. **55**, 2078 (1984).

[3] J. F. Herbst, J. J. Croat, F. E. Pinkerton, and W. B. Yelon, Phys. Rev. B **29**, 4176 (1984).

[4] Xue-Fu Zhong and W. Y. Ching, Phys. Rev. B **39**, 12018 (1989).

[5] J. F. Herbst, Rev. Mod. Phys. **63**, 819 (1991).

[6] D. Haskel, J. C. Lang, Z. Islam, A. Cady, G. Srajer, M. van Veenendaal, and P. C. Canfield, Phys. Rev. Lett. **95,** 217207 (2005).

[7] E. B. Boltich, E. Oswald, M. Q. Huang, S. Hirosawa, and W. E. Wallace, J. Appl. Phys. **57**, 4106 (1985).

[8] S. Hirosawa, Y. Matsuura, H. Yamamoto, S. Fujimura, and M. Sagawa, J. Appl. Phys. **59**, 873 (1986).

[9] M. Sagawa, S. Fujimura, H. Yamamoto, Y. Matsuura, and K. Hiraga, IEEE Trans. Magnetics **20**, 1584 (1984).

[10] R. Fischer, T. Leineweber, and H. Kronmüller Phys. Rev. B **57**, 10723 (1998).

[11] T. Schrefl, J. Fidler, and H. Kronmüller, Phys. Rev. B **49**, 6100 (1994).

[12] D. W. Lim, H. Kato, M. Yamada, G. Kido, and Y. Nakagawa, Phys. Rev. B**44**, 10014 (1991).

[13] A. Yasui, T. Nakamura, Y. Kotani, T. Fukagawa, T. Nishiuchi, and S. Hirosawa, J. Appl. Phys. **117**, 17B313 (2015).

[14] T. Nakamura, A. Yasui, Y. Kotani, T. Fukagawa, T. Nishiuchi, H. Iwai, T. Akiya, T. Ohkubo, Y. Gohda, K. Hono, and S. Hirosawa, Appl. Phys. Lett. **105**, 202404 (2014).

[15] T. Miyake and H. Akai, J. Phys. Soc. Jpn. **87**, 041009 (2018)

[16] M. Yamada, H. Kato, H. Yamamoto, and Y. Nakagawa, Phys. Rev. B**38**, 620 (1988).

[17] J. Kamarad, Z. Arnold, and J. Schneider, J. Magn. Magn. Mater. **67**, 29 (1987).

[18] K. Fukamachi, K. Shirakawa, Y. Satoh, T. Masumoto, and T. Kaneko, J. Magn. Magn. Mater. **54–57**, 231 (1986).

[19] M. Mito, H. Goto, K. Nagai, K. Tsuruta, H. Deguchi, T. Tajiri, and K. Konishi, J. Appl. Phys. **118**, 145901 (2015).

[20] B. I. Min, J.-S. Kang, J. H. Hong, J. I. Jeong, Y. P. Lee, S. D. Choi, W. Y. Lee, C. J. Yang, and C.

G. Olson, Phys. Rev. B **48**, 6217 (1993).

[21] T. Varga, A. P. Wilkinson, and R. J. Angel, Rev. Sci. Instrum. **74**, 4564 (2003).

[22] G. J. Piermarini, S. Block, J. D. Barnett, and R. A. Forman, J. Appl. Phys. **46**, 2774 (1975).

[23] F. Izumi and K. Momma, Solid State Phenom., **130** (2007) 15.

[24] Q.Y. Li, S.C. Shi, J.W. Yang, and Y. Sun, Chinese Journal of High Pressure Physics **21**, 210 (2007).

Table I. Structural parameters after the Rietveld refinement of XRD pattern at ambient pressure. The space group is $P4_2/mnm$. Atomic position of Fe6 is at 4*c* (0, 1/2, 0). The Rietveld analysis for the XRD pattern is converged with an *R* factor, R_{wp} = 6.957 and R_e = 2.535.

Lattice	*a* [Å]	*c* [Å]	*V* [Å^3]
constants	8.7570(2)	12.1512(6)	931.81(6)

Atom	Site	*x*	*y*	*z*
Nd1	4*g* *x -x* 0	0.2309(3)	-0.2309(3)	0
Nd2	4*f* *x x* 0	0.3577(3)	0.3577(3)	0
Fe1	16*k* *x y z*	0.0388(5)	0.3585(7)	0.3242(5)
Fe2	16*k* *x y z*	0.0697(6)	0.2770(6)	0.1306(5)
Fe3	8*j* *x x z*	0.0966(6)	0.0966(6)	0.2979(5)
Fe4	8*j* *x x z*	0.3179(5)	0.3179(5)	0.2531(6)
Fe5	4*e* 0 0 *z*	0	0	0.1179(10)
B	4*f* *x x* 0	0.148(5)	0.148(5)	0

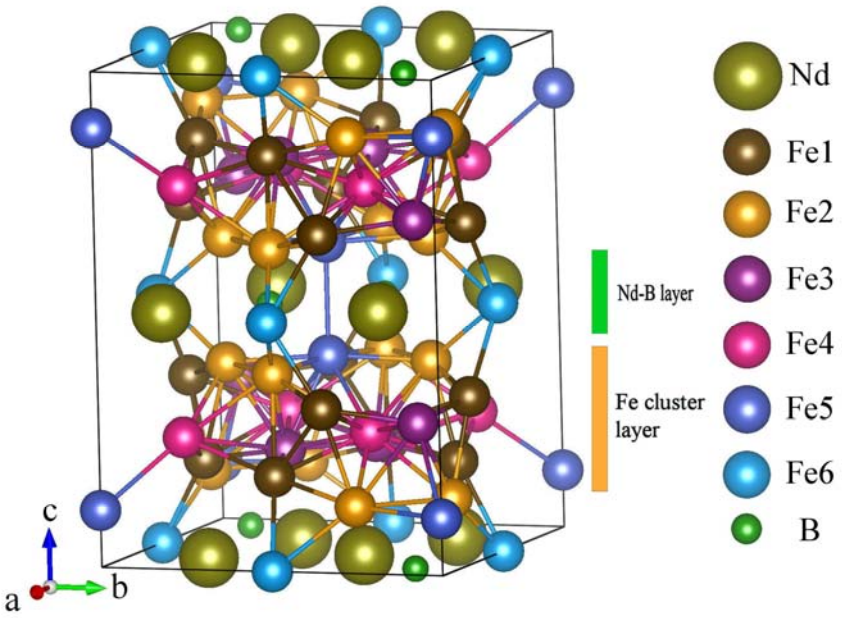

Fig. 1. Crystal structure of $Nd_2Fe_{14}B$. All Nd and B atoms and the Fe6 site reside in the z = 0 and 0.5 planes. Between these planes, other Fe sites (Fe1 – Fe5) form somewhat distorted connected hexagonal nets as shown in Fig. 6 (a).

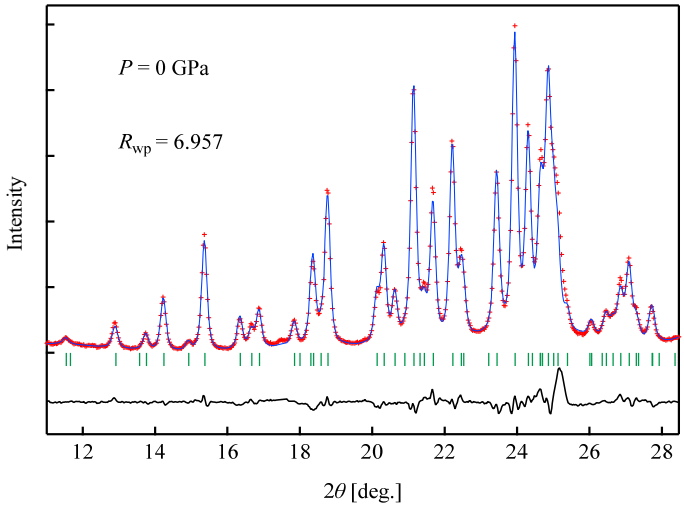

Fig. 2. Powder XRD pattern of $Nd_2Fe_{14}B$ at ambient pressure. The incident X-ray wavelength was 0.88249 Å. The red symbol, the blue and black curves, and the green bar represent experimental data, fitting curve, and deviation between experimental data, analytic data, and Bragg angle position for $Nd_2Fe_{14}B$ crystal, respectively.

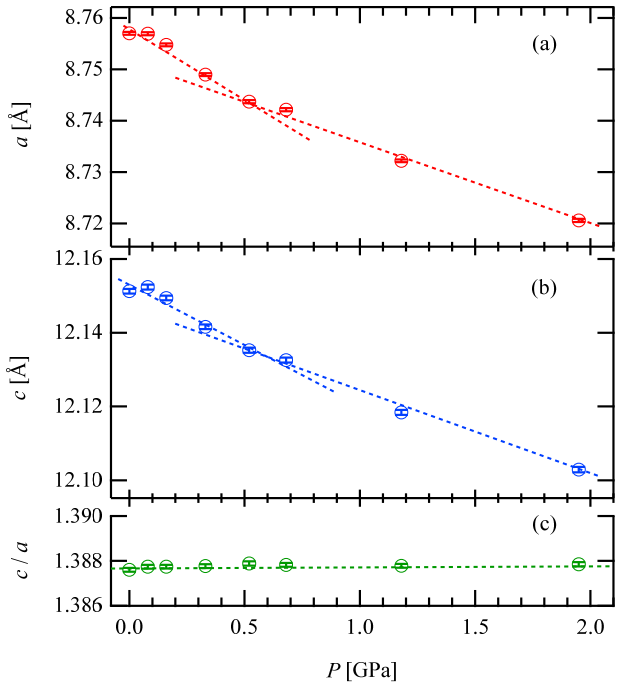

Fig. 3. Pressure dependence of lattice constants *a* (a) and *c* (b) for $Nd_2Fe_{14}B$ at room temperature. (c) Ratio of lattice constants *c* to *a* as a function of pressure.

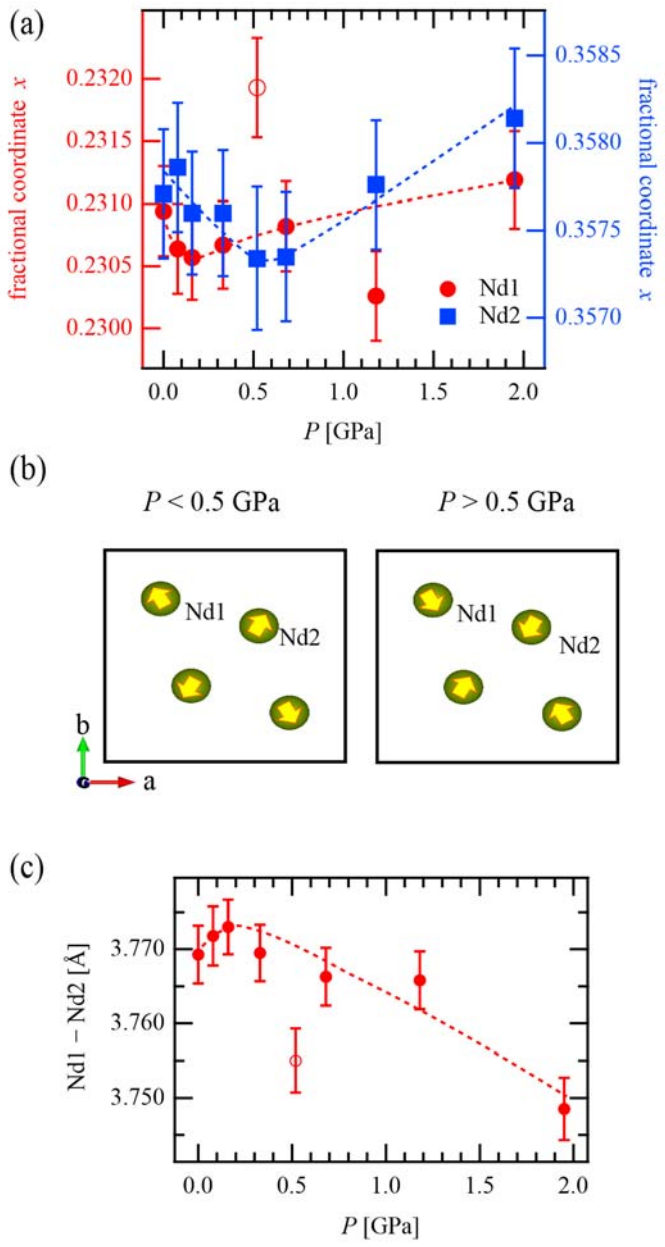

Fig. 4. (a) Pressure dependence of the atomic position for two Nd sites: Nd1(x, -x, 0) and Nd2(x, x, 0). (b) Schematics of displacement of Nd atoms in the *ab*-plane within one unit cell. (c) Pressure dependence of the bond distances between Nd atoms.

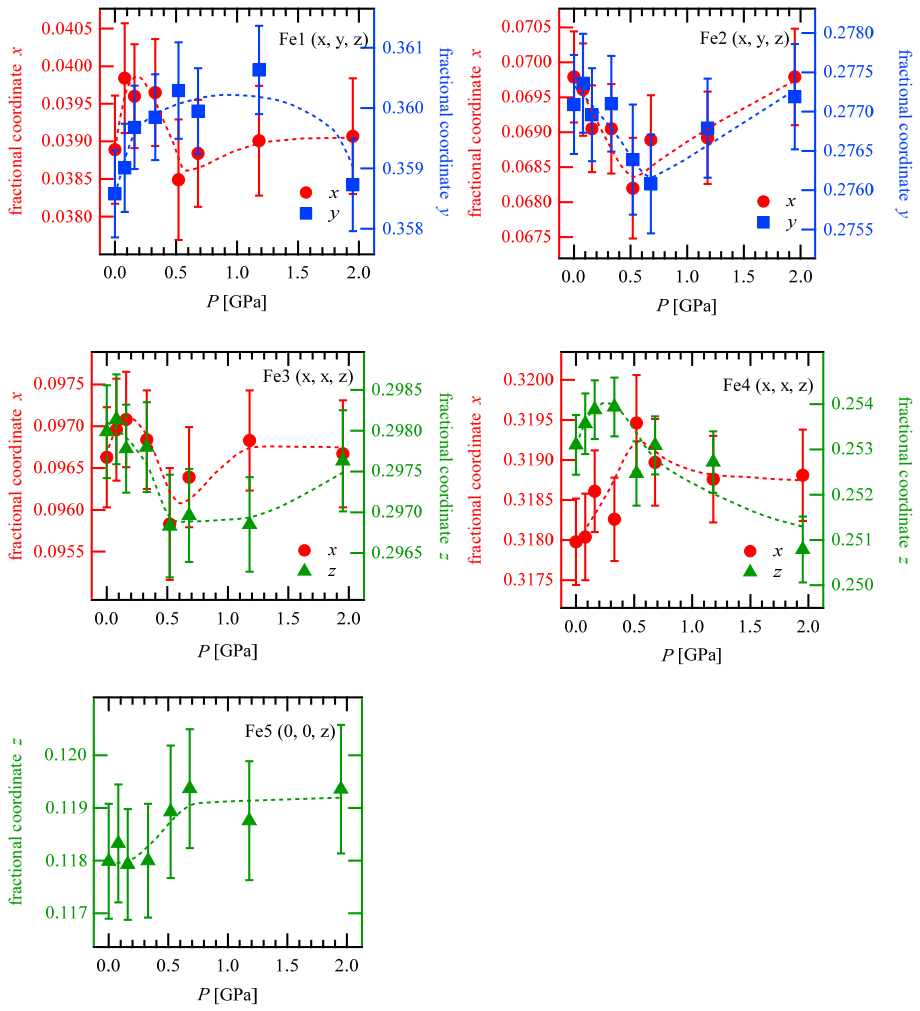

Fig. 5. Pressure dependence of the atomic position for five Fe sites: Fe1(x, y, z) (a), Fe2(x, y, z) (b), Fe3(x, x, z) (c), Fe4(x, x, z) (d), and Fe5(0, 0, z) (e).

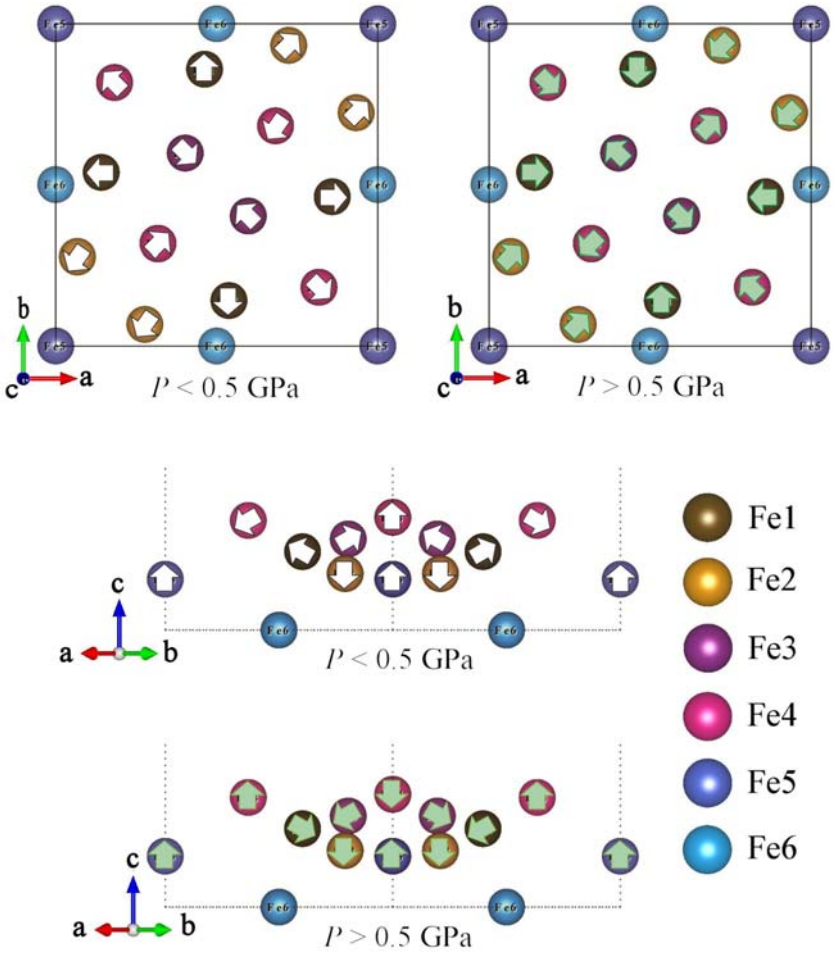

Fig. 6. Schematic views of the displacement of Fe atoms in an *ab*-plane projection (a, b) within one unit cell and (110) plane projection (c, d) within one unit cell. Arrows represent the direction of displacement of each atom. The dotted line in the *ab*-plane projection show a hexagonal Fe net.

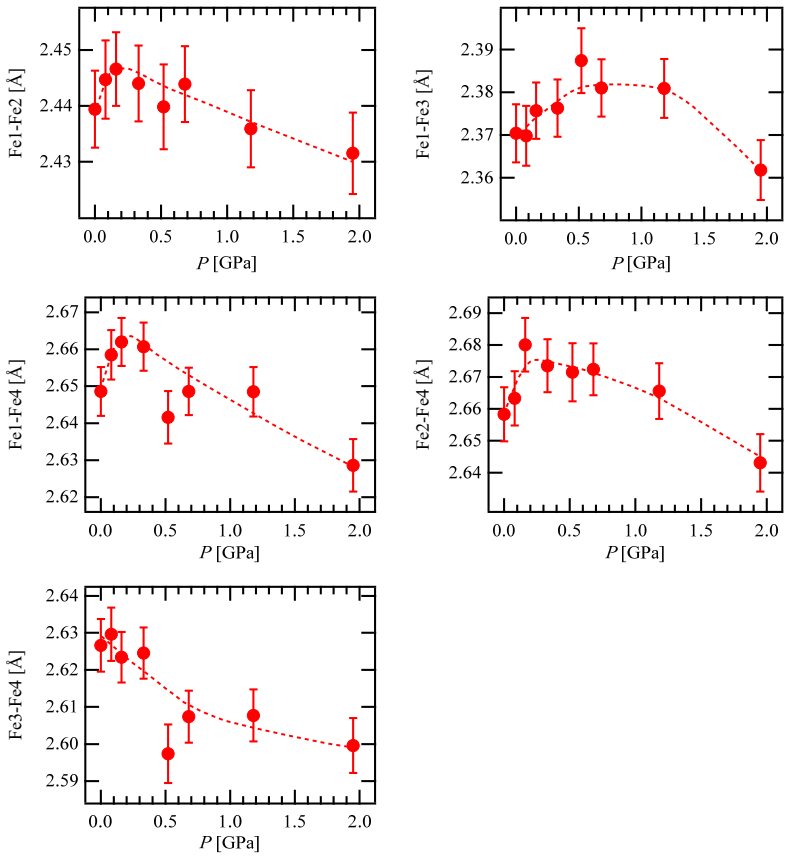

Fig. 7. Pressure dependence of the representative interatomic distances between different Fe sites around Nd sites.

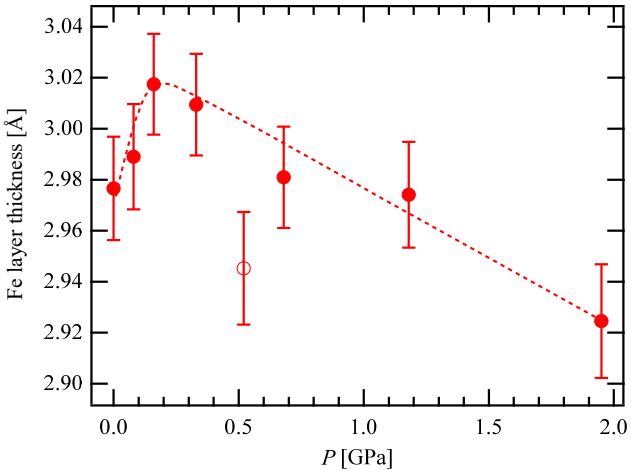

Fig. 8. Pressure dependence of thickness of Fe cluster layer in a unit cell.

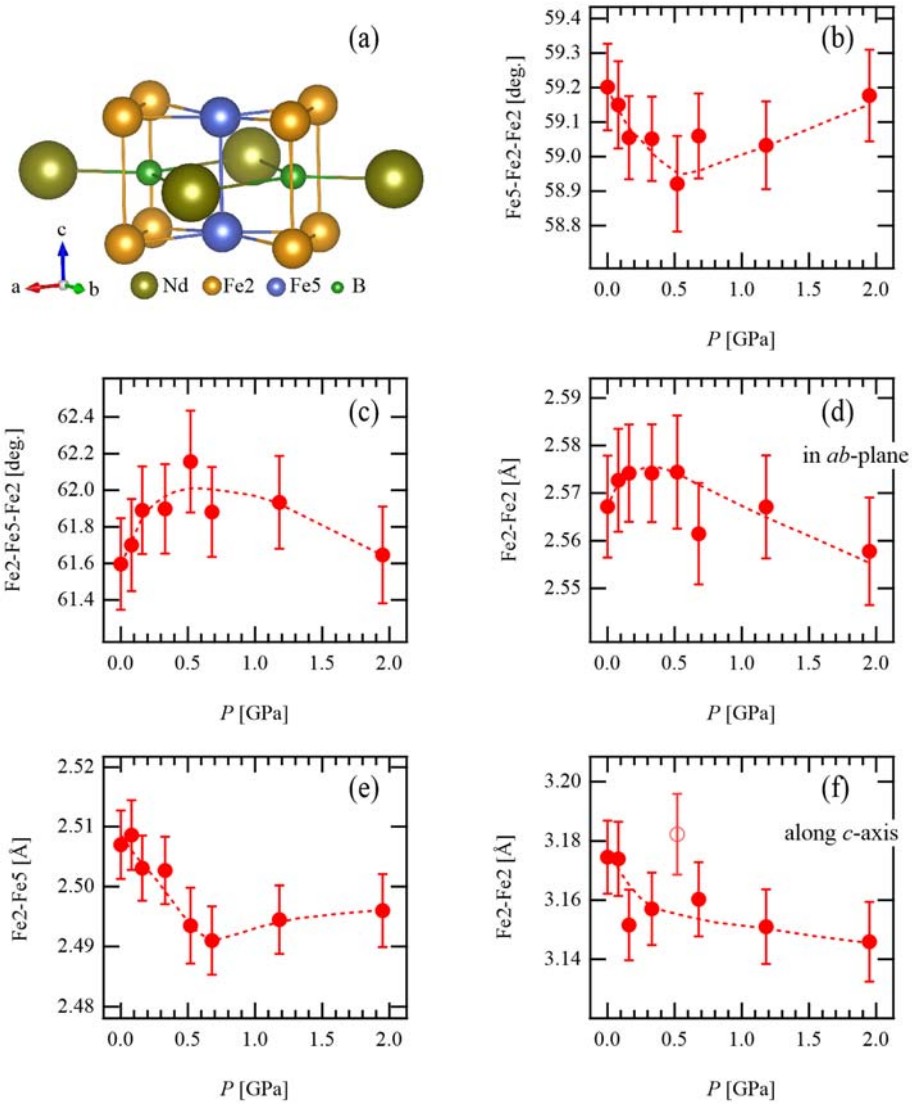

Fig. 9. (a) Trigonal prism formed by Fe atoms (Fe2 and Fe5) containing a B atom in the Fe layers. The pressure dependences of (b, c) bond angles and (d, e, f) distances between neighboring Fe atoms.

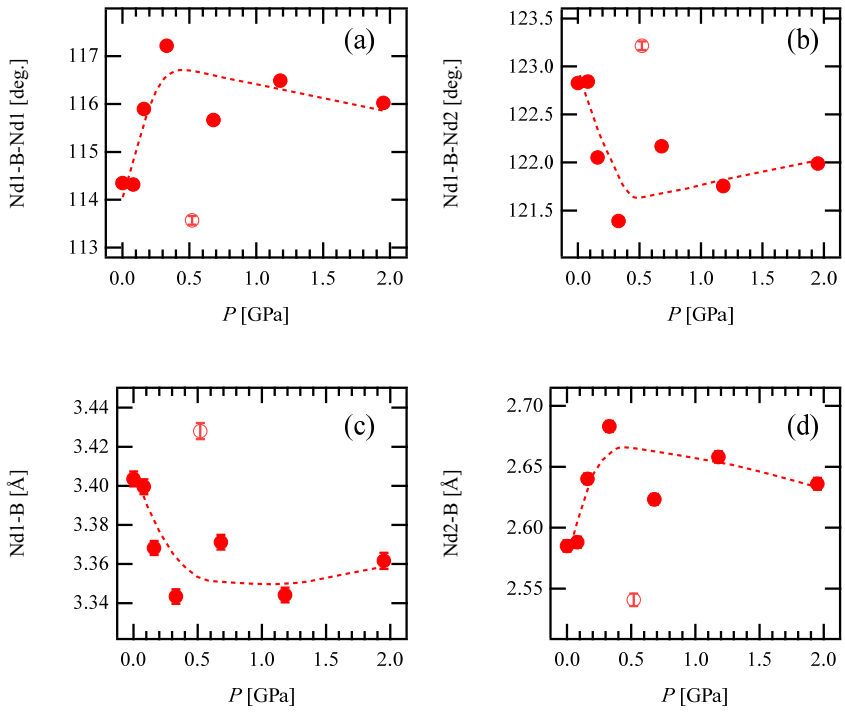

Fig. 10. Pressure dependence of (a, b) bond angles and (c, d) distances between Nd and B atoms around a trigonal prism, as shown in Fig. 9(a).

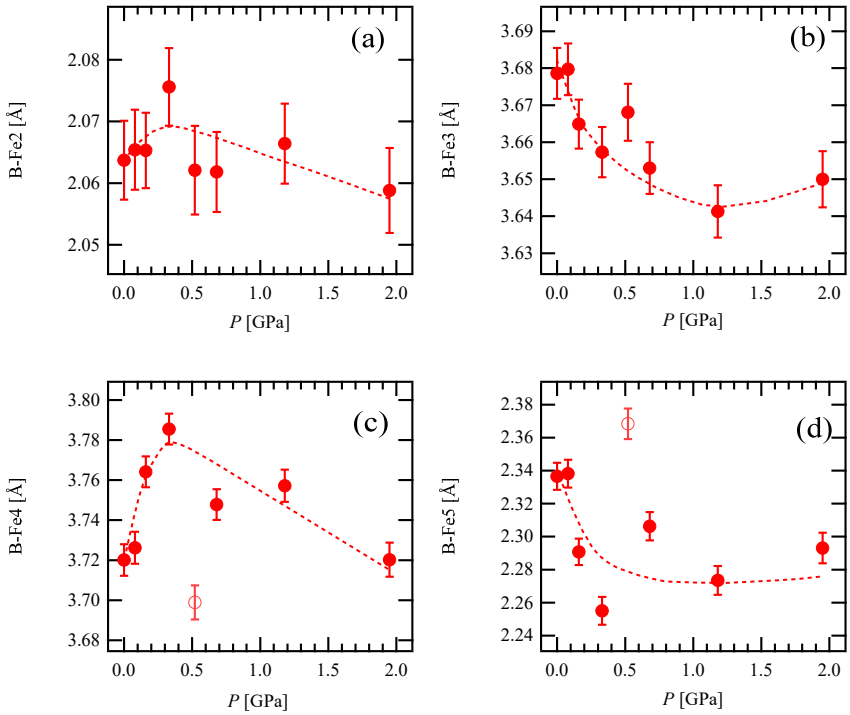

Fig. 11. Pressure dependence of distances between B and Fe atoms.